fraction of the area's biotopes, the total number of which by far exceeds 100. Inadequate sampling of different biotopes leads to erroneous conclusions on the distribution of species and the conservation value of different areas. Furthermore, underrepresentation of β-diversity may explain the relatively low γ-diversity reported for the area (5). Therefore, in studies like national biodiversity assessments it is imperative to take the limits of ecologically comparable patches into account when planning biological field research and extrapolating the results. Reliable spatial data, such as maps of vegetation and soil properties, are urgently needed for precise hypothesis formulation and testing in ecology and biogeography and for directing conservation efforts to preserve representative environments from different regions.

REFERENCES AND NOTES

1. K. R. Young and B. León, *Brittonia* **41**, 388 (1989).
2. H. Tuomisto and K. Ruokolainen, *J. Veg. Sci.* **5**, 25 (1994).
3. T. L. Erwin, *Coleopt. Bull.* **36**, 74 (1982); J. W. Terborgh, J. W. Fitzpatrick, L. Emmons, *Fieldiana Zool.* **21**, 1 (1984); H. Balslev, J. Luteyn, B. Øllgaard, L. B. Holm-Nielsen, *Opera Bot.* **92**, 37 (1987); A. H. Gentry, *Proc. Natl. Acad. Sci. U.S.A.* **85**, 156 (1988); R. Valencia, H. Balslev, G. Paz y Miño, *Biodivers. Conserv.* **3**, 21 (1994).
4. A. H. Gentry, *Ann. Mo. Bot. Gard.* **75**, 1 (1988).
5. S. S. Renner, H. Balslev, L. B. Holm-Nielsen, *AAU Reports* **24**, 1 (1990); L. Brako and J. L. Zarucchi, *Monogr. Syst. Bot. Mo. Bot. Gard.* **45**, 1 (1993).
6. F. Encarnación, *Candollea* **40**, 237 (1985); G. T. Prance, in *Ecosystems of the World,* vol. 14B, *Tropical Rain Forest Ecosystems: Biogeographical and Ecological Studies*, H. Lieth and M. J. A. Werger, Eds. (Elsevier, Amsterdam, 1989).
7. J. A. Endler, *Geographic Variation, Speciation, and Clines* (Princeton Univ. Press, Princeton, NJ, 1977).
8. A. H. Gentry, *Plant Syst. Evol.* **137**, 95 (1981); J. F. Duivenvoorden and J. M. Lips, *Landscape Ecology of the Middle Caquetá Basin* (Studies on the Colombian Amazonia, Tropenbos, Colombia, 1993), vol. IIIA.
9. P. Legendre and A. Vaudor, *The R Package: Multidimensional Analysis, Spatial Analysis* (Département de Sciences Biologiques, Université de Montréal, Montreal, Canada, 1991).
10. H. Tuomisto, A. Linna, R. Kalliola, *Int. J. Remote Sens.* **15**, 1595 (1994).
11. R. Kalliola, M. Puhakka, W. Danjoy, Eds., *Amazonia Peruana—Vegetación Húmeda Tropical en el Llano Subandino* (PAUT y ONERN, Jyväskylä, Finland, 1993).
12. R. Kalliola, M. Puhakka, J. Salo, H. Tuomisto, K. Ruokolainen, *Ann. Bot. Fennici* **28**, 225 (1991); H. Tuomisto, R. Kalliola, K. Ruokolainen, A. Linna, unpublished data.
13. K. Ruokolainen, H. Tuomisto, R. Ríos, A. Torres, M. García, *Acta Amazonica*, in press; K. Ruokolainen and H. Tuomisto, unpublished data.
14. M. Puhakka, R. Kalliola, M. Rajasilta, J. Salo, *J. Biogeogr.* **19**, 651 (1992).
15. W. J. Junk, in *The Amazon. Limnology and Landscape Ecology of a Mighty Tropical River and Its Basin*, H. Sioli, Ed. (Junk, Dordrecht, Netherlands, 1984), pp. 215–243; K. Kubitzki, *Plant. Syst. Evol.* **162**, 285 (1989); D. G. Campbell, D. C. Daly, G. T. Prance, U. N. Maciel, *Brittonia* **38**, 369 (1986); J. D. Mitchell and S. A. Mori, *Mem. N.Y. Bot. Gard.* **44**, 113 (1987).
16. H. ter Steege, V. G. Jetten, A. M. Polak, M. J. A. Werger, *J. Veg. Sci.* **4**, 705 (1993).
17. J. Salo *et al.*, *Nature* **322**, 254 (1986).
18. M. E. Räsänen, J. S. Salo, R. Kalliola, *Science* **238**, 1398 (1987); M. Räsänen, R. Neller, J. Salo, H. Jungner, *Geol. Mag.* **129**, 293 (1992); C. Hoorn, *Paleogeogr., Paleoclimatol., Paleoecol.* **105**, 267 (1993).
19. I. Hanski, *Trends Ecol. Evol.* **4**, 113 (1989); D. S. Wilson, *Ecology* **73**, 1984 (1992); D. A. Levin, *Syst. Bot.* **18**, 197 (1993).
20. A. Shmida and M. V. Wilson, *J. Biogeogr.* **12**, 1 (1985); S. P. Hubbell and R. B. Foster, in *Community Ecology*, J. Diamond and T. J. Case, Eds. (Harper & Row, New York, 1986), pp. 314–329.
21. J. Haffer, *Science* **165**, 131 (1969); G. T. Prance, Ed., *Biological Diversification in the Tropics* (Columbia Univ. Press, New York, 1982); J. Haffer, *Biogeographica* **69**, 15 (1993).
22. P. Hershkovitz, *Evolution* **22**, 556 (1968).
23. S. A. Mori and G. T. Prance, *Mem. N.Y. Bot. Gard.* **44**, 55 (1987).
24. Workshop 90, *Biological Priorities for Conservation in Amazonia* (Conservation International, Washington, DC, 1991).
25. B. W. Nelson, C. A. Ferreira, M. F. da Silva, M. L. Kawasaki, *Nature* **345**, 714 (1990).
26. R. Spichiger, J. Méroz, P.-A. Loizeau, L. Stutz de Ortega, *Boissiera* **43**, 1 (1989); R. Spichiger, J. Méroz, P.-A. Loizeau, L. Stutz de Ortega, *ibid.* **44**, 1 (1990).
27. SYSTAT, Inc., *SYSTAT: Statistics, Version 5.2 Edition* (Evanston, IL, 1992).

28. Dedicated to the memory of Alwyn H. Gentry, whose pioneering work in neotropical floristics and biogeography has greatly inspired us. We thank D. Borcard, S. Kroonenberg, R. C. Moran, A. D. Poulsen, M. Räsänen, and J. Salo for constructive comments on the manuscript. Supported by the Academy of Finland and FINNIDA.

15 November 1994; accepted 23 March 1995

Interaction of a Peptidomimetic Aminimide Inhibitor with Elastase

Ezra Peisach, David Casebier, Steven L. Gallion, Paul Furth, Gregory A. Petsko, Joseph C. Hogan Jr., Dagmar Ringe*

The crystal structure of an aminimide analog of a dipeptide inhibitor of porcine pancreatic elastase bound to its target serine protease has been solved. The peptidomimetic molecule binds in the same fashion as the class of dipeptides from which it was derived, making similar interactions with the subsites on the elastase surface. Because aminimides are readily synthesized from a wide variety of starting materials, they form the basis for a combinatorial chemistry approach to rational drug design.

Drug discovery begins with the identification of a lead compound, usually a peptide, that possesses activity against the desired target. Often, target macromolecules are proteases, and their peptide substrates provide obvious leads. This is true for protein kinases and phosphatases and receptors for which naturally occurring peptide agonists or antagonists are known. Phage display (*1*) and other methods (*2*) for generating and screening large libraries of peptide sequences make it easy to identify small peptide sequences that have micromolar affinity for most protein targets, even those that do not normally bind peptides. Modifications are often necessary to improve a lead compound's physical and biochemical properties. Recently, attempts have been made to develop peptidomimetic compounds that have backbone structures similar but superior to those of peptides.

Aminimides **2** are a class of peptidomimetics that are hydrazinium hydroxide inner salts. Aminimides are stable under both acidic and basic conditions and are resistant to proteolytic attack. The zwitterionic nature of aminimides enhances their solubility in protic, aprotic, and nonpolar media (*3*); these compounds are chiral because of their quaternary hydrazinium centers. Oligomers based on aminimide linkages can be synthesized readily. Such compounds have an additional atom in their backbone but may be able to interact with proteins like statine-based inhibitors (which have two additional backbone atoms per statine residue) or like hydrazino peptides (which have one) (*4*).

To determine how aminimide linkages affect side chain and main chain interactions with the active site of a target enzyme, we inhibited the serine protease elastase with an aminimide inhibitor based on a trifluoroacetyl (TFA) dipeptide and determined the structure of the complex at high resolution by x-ray diffraction. Trifluoroacetyl dipeptide anilides are potent, reversible inhibitors of porcine pancreatic elastase. Their inhibition constants (K_i's) are in the low micromolar range; a number of different dipeptide sequences have been synthesized and characterized (*5*).

We have developed here a paradigm for structure-based drug design in which the complete binding surface of the target protein is mapped by crystal structure studies in a variety of organic solvents, followed by combinatorial chemistry to identify and im-

E. Peisach, Program in Biophysics, Brandeis University, Waltham, MA 02254, USA.
D. Casebier, S. L. Gallion, P. Furth, J. C. Hogan Jr., ArQule, 200 Boston Avenue, Medford, MA 02155, USA.
G. A. Petsko and D. Ringe, Departments of Biochemistry and Chemistry and Rosenstiel Basic Medical Sciences Research Center, Brandeis University, Waltham, MA 02254, USA.

*To whom correspondence should be addressed.

prove lead compounds directed at the identified sites (6). Like other serine proteases, elastase possesses an extended substrate binding site, composed of a set of pockets along the crevice formed by a domain interface (7). As many as five substrate residues can be accommodated along this cleft on the COOH-terminal side of the scissile bond, with an additional two or more subsites thought to occur on the leaving-group side. For elastase, solvent mapping identifies four primary target locations on the acyl side of the catalytic triad. Three of these (S1, S2, and S3) are normally occupied by the side chains of amino acids in peptide inhibitors. The fourth subsite is potentially available for exploitation by inhibitors with multiple heads.

Using information from inhibited complexes of elastase and solvent mapping, we designed a peptidomimetic inhibitor to mimic the dipeptide TFA-Leu-Phe-Iso. (where Iso. is *p*-isopropylanilide) (**1**) by modification of Phe to contain an aminimide linkage. The new inhibitor TFA-Leu-MBA-Iso. {TLMI; where MBA is methyl benzyl aminimide [1-benzyl-1-methyl-1-(2-acetyl)-hydrazinium hydroxide salt]} (**2**) demonstrated both increased solubility and inhibition relative to the parent dipeptide (8). The TLMI inhibitor had a K_i value of 26 μM, whereas the dipeptide at maximum solubility (approximately 20 μM) did not inhibit elastase at all (9).

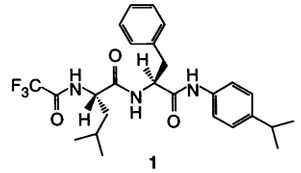

1

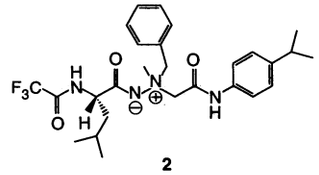

2

Crystals of porcine pancreatic elastase (PPE) were grown, and the aminimide inhibitor TLMI was soaked in as described (*10*). Attempts to cocrystallize or soak the dipeptide inhibitor **1** into PPE were unsuccessful because of the low solubility of this inhibitor. Crystals of the TLMI-elastase complex are orthorhombic, with space group $P2_12_12_1$ with one molecule in the asymmetric unit, and are isomorphous with those of uninhibited PPE and of PPE with similar dipeptide inhibitors bound (a = 52.16 Å, b = 57.68 Å, and c = 75.52 Å) (Table 1) (*11*, *12*). The refined structure (final R factor of 19.2% to 1.8 Å resolution) of the PPE-aminimide inhibitor complex shows the inhibitor bound in the active site. Both the initial and final electron density maps are easy to interpret (*13*).

Porcine pancreatic elastase is a monomer of 240 amino acids with two domains (*7*). It has the classical serine protease catalytic triad of an aspartic acid, a histidine, and the eponymous serine. The overall structure of the protein in the complex is the same as that of uninhibited elastase, with the following differences. The final electron density map clearly shows an alternate conformation for the side chain of Arg^{226} (*14*), as seen in some other inhibited elastase structures (*11*). This side chain was refined with 50% occupancy in the original and new conformations. A calcium ion and a sulfate ion were found at positions previously reported; however, the sulfate ion that is often found in the active site in native structures was absent (*11*). There are no other conformational changes in side chains relative to the uninhibited PPE structure.

Figure 1 shows the fit of the aminimide inhibitor to the electron density in the active site. Other structures of noncovalent TFA dipeptide inhibitor elastase complexes reveal that the inhibitors bind in several modes (*11*, *15*, *16*). In all cases, these inhibitors bind to elastase in the reverse orientation relative to that expected for substrates by forming a hydrogen-bonded parallel sheet with the side of the active site. Like these inhibitors, the aminimide inhibitor is situated in the active site on the acyl group side underneath the catalytic triad. For instance, it binds in the same orientation and in the same subsites as the dipeptide inhibitor TFA-Leu-Ala-trifluoromethyl anilide (TFLA) (*17*), except for the MBA residue. The benzyl side chain of the MBA residue lies in the pocket where the Iso. group of the TFA-Lys-Phe-Iso. (TFKF) dipeptide inhibitor (*15*) is found, thereby taking advantage of a potentially available alternate mode. In essence, this aminimide

Table 1. Refinement of PPE with the TLMI inhibitor. Diffraction data were collected on a Siemens X100-A multiwire area detector mounted on an Eliot GX-6 rotating anode generator operating at 24 kV and 25 mA with the use of Ni-filtered Cu Kα radiation. Data were taken at room temperature, with an oscillation angle of 0.2° and 450 s per frame. A full 90° of data were collected, and a subsequent 84° taken perpendicular to the original orientation. The program XDS (*18*) was used to process and analyze the data, and the program XSCALE (*18*) was used to merge the data from the two orientations. *I*, intensity.

Total reflections (n)	44,505
Unique reflections (n) ($I/\sigma(I) > 0$)	39,545
Completeness of data to 1.8 Å (%)	58.7
R_{merge}* (%)	6.3
Correlation between intensities of common reflections	98.3%
Resolution range (Å)	10–1.8
R_{factor}† (%)	19.2
Water molecules (n)	134
B values (Å^2)	
Main chain	14.7
Side chains	19.4
Inhibitor	40.4
Waters	31.8
Deviations observed	
rms, bond lengths (Å)	0.015
rms, bond angles (degrees)	2.7
rms, planar groups) (Å)	1.0

*$R_{merge} = \Sigma|I_o - I_a|/\Sigma(I_a)$ (where I_o is the observed intensity and I_a is the average intensity), the sums being taken over all symmetry-related reflections. †$R_{factor} = \Sigma|F_o - F_c|/\Sigma(F_o)$, the sums being taken over all reflections.

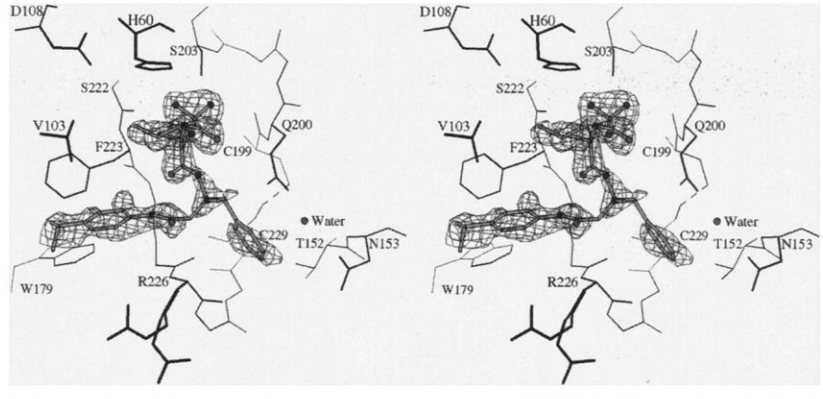

Fig. 1. Stereo view of the aminimide inhibitor in the active site of PPE (*19*). The catalytic triad is viewed horizontally with the extended substrate binding cleft running vertically downward. The backbone of peptide substrates forms an antiparallel β sheet with segments of the enzyme that line the crevice (residues 222 to 224). This arrangement directs alternate substrate side chains to opposite sides of the cleft. Thus, the PI specificity pocket is located just below and to the right of Ser^{203}. The P2 binding pocket is to the left, underneath His^{60}. Continuing the alternation of sites, P3 is located further down, on the right side of the crevice. The electron density shown is for the inhibitor only at the 0.8σ level. Side chains of the residues of the catalytic triad (Asp^{108}, His^{60}, and Ser^{203}) and selected residues around the active site region mentioned in the text are shown. The side chain of Arg^{226} is shown in two conformations, which appear with approximately equal occupancy. The figure was rendered with the use of MOLSCRIPT (*20*).

interacts with subsites on the enzyme that have been observed in two separate dipeptide inhibitors and is therefore a hydra-headed inhibitor using multiple binding modes simultaneously (Fig. 2).

The TFA group of the aminimide inhibitor binds in the vicinity of the oxyanion hole in the S1 subsite (Fig. 3). The electron density for the CF_3 group is well defined, and distinct lobes are observed for the three fluorine atoms as in the structures of the TFLA inhibitor and the TFA-Lys-X-Iso. inhibitor complexes (where X is Leu, Phe, and Pro) (*11*). Two fluorine atoms are 3.1 Å from the catalytic Oγ of Ser^{203}. This Ser hydroxyl accepts a hydrogen bond (2.8 Å) from His^{60}. One fluorine atom is also 3.2 Å from the backbone nitrogen of Ser^{203}. The carbonyl oxygen of the TFA group is in van der Waals contact (3.6 Å) with the backbone nitrogen of Gln^{200}. These distances are similar to those observed in structures of elastase complexes with analogous dipeptide inhibitors (*11*, *17*).

The leucine side chain of the aminimide inhibitor is situated in the S2 subsite. The backbone nitrogen of this residue makes two hydrogen bonds: to Oγ of Ser^{203} (3.2 Å) and to the backbone carbonyl of Ser^{222} (3.1 Å). The carbonyl oxygen at this inhibitor side chain accepts a hydrogen bond from the backbone nitrogen of Val^{224} (2.9 Å). The entire side chain of this leucine is in good electron density, and the tip of the side chain is clearly visible. In the structure of an analogous dipeptide inhibitor complex, PPE-TFLA (*17*), the two terminal methyl groups of the side chain are rotated 120° around the Cβ–Cγ bond, which moves the side chains of His^{60} and Ser^{203} out of the way. In the aminimide complex structure, there are hydrophobic interactions between the leucine side chain and the imidazole ring of His^{60}. Neither His^{60} nor Ser^{203} moved from its native position in this complex. Such interactions are observed in all TFA dipeptide inhibitors that have an aliphatic group in this position (*11*).

The MBA residue, which is the aminimide analog of Phe in the TFA-Leu-Phe-Iso. dipeptide inhibitor, is located near the S3 subsite. The hydrazinium hydroxide internal salt lacks the amide hydrogen and therefore cannot form a hydrogen bond with any of the surrounding protein matrix as similar dipeptide inhibitors do. The extra atom at this position causes the backbone of the inhibitor to bulge out slightly away from the surface as was predicted by simple conformational analysis of aminimide models. This bulge has no effect on the interactions of the side chains of the inhibitor with the appropriate pockets on the enzyme surface. The methyl side chain, which determines the chirality of this residue, is positioned trans to the planar carbonyl-aminimide linkage. This conformation is energetically favored and gives a better fit to the observed electron density in this region. The aminimide linkage shows clearly in the electron density maps. The benzyl part of the MBA residue points toward a pocket that is more hydrophilic than hydrophobic. The pocket is lined with the side chains of Asn^{153}, Gln^{200}, and a water molecule on one side and the backbones of residues 226 to 229 on the other. The lack of strong interactions with the protein could therefore contribute to the relatively poor electron density and high temperature factors seen for this side chain. Electron density in this region is also poor for analogous peptides, which have similar high temperature factors (*11*). The orientation of the benzyl group corresponds to that of the isopropyl anilide functional group in the dipeptide inhibitor complex TFA-Lys-Phe-Iso., in which the orientation of the inhibitor is shifted down relative to TFLA.

The isopropyl anilide, in the putative S4 subsite, is held in place with a hydrogen bond (3.4 Å) between its nitrogen and the carbonyl oxygen of Val^{224}. This same interaction was observed in dipeptide inhibitors that have an Iso. group in this subsite. In addition, hydrophobic contacts were observed between the anilide ring and the side chains of Trp^{179}, Phe^{223}, and Val^{103}, as in complexes of PPE with other dipeptide anilide inhibitors.

The aminimide molecule is a competitive inhibitor of PPE with a K_i value in the low micromolar range, similar to that of the class of corresponding dipeptide inhibitors. In contrast to the dipeptide that is its closest analog (TFA-Leu-Phe-Iso.), the aminimide inhibitor is soluble in aqueous solutions at concentrations much greater than its K_i value. In fact, the dipeptide inhibitor is so insoluble in aqueous media that its K_i cannot be determined. We found that the

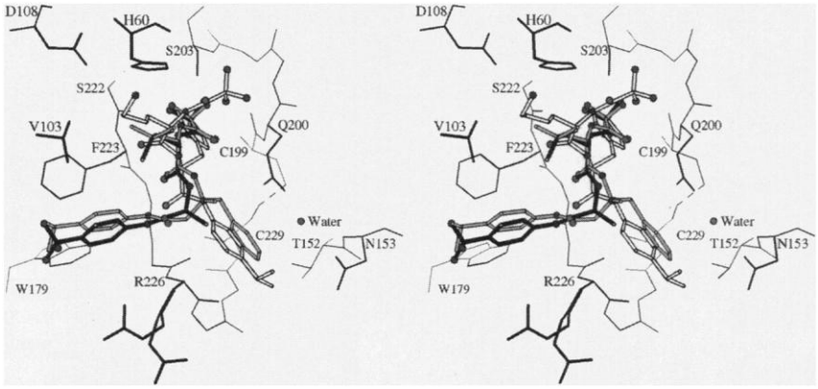

Fig. 2. Stereo view of the active site of PPE with the positions of the aminimide inhibitor (gray), TFA-Leu-Ala-TFM (where TFM is *p*-trifluoromethylanilide) (black) (Brookhaven Protein Databank entry code 8est), and TFA-Lys-Phe-Iso. (white) (*19*). The view of the active site is the same as for that of Fig. 1. Note that the backbones of the aminimide inhibitor and TFA-Leu-Ala-TFM practically superimpose. The aminimide inhibitor takes advantage of two binding subsites in a hydra-headed manner, which were originally observed individually with the TFA-Leu-Ala-TFM and TFA-Lys-Phe-Iso. inhibitor complexes. Thus, the isopropyl anilide group of the aminimide inhibitor binds in the same subsite of the methyl anilide (black), and the benzyl group of the aminimide binds in the same subsite of the Iso. group of the inhibitor (white). The figure was rendered with MOLSCRIPT (*20*).

Fig. 3. Schematic diagram of the aminimide inhibitor bound to PPE. Distances indicated are in angstroms.

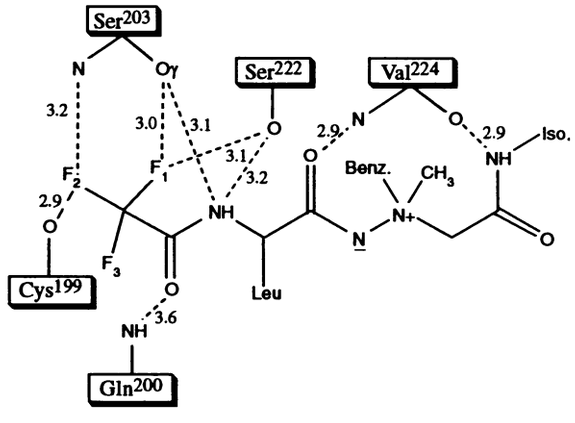

aminimide inhibitor was able to make nearly all the interactions with the enzyme that corresponding dipeptide inhibitors make. Although the aminimide contains an extra backbone atom relative to conventional amino acids, the carbonyl groups of the peptidomimetic make the same hydrogen bonds, and the side chains of the aminimide dipeptide analog bind to the same subsites on the enzyme.

REFERENCES AND NOTES

1. S. E. Cwirlay, E. A. Peters, R. W. Barrett, W. J. Dower, *Proc. Natl. Acad. Sci. U.S.A.* **87**, 6378 (1990); J. J. Devlin, L. C. Panganiban, P. E. Devlin, *Science* **249**, 404 (1990).
2. J. K. Scott and G. P. Smith, *Science* **249**, 386 (1990); H. M. Geysen, S. J. Rodda, T. J. Mason, Eds., *CIBA Found. Symp.* **119** (1986); M. A. Gallop, R. W. Barret, W. J. Downer, S. P. Fodor, E. M. Gordon, *J. Med. Chem* **37**, 1233 (1994).
3. D. Ringe, unpublished results.
4. A. Amour, A. Collet, C. Dubar, M. Reboud-Ravaux, *Int. J. Peptide Protein Res.* **43**, 297 (1994); A. Aubury *et al.*, *ibid.*, p. 305.
5. D. L. Hughes, L. C. Sieker, J. Beith, J.-L. Dimicoli, *J. Mol. Biol.* **162**, 645 (1982); A. Renaud, P. Lestienne, D. L. Hughes, J. Bieth, J.-L. Dimicoli, *J. Biol. Chem.* **258**, 8312 (1983).
6. D. Ringe and G. A. Petsko, in *New Perspectives in Drug Design*, P. M. Dean, G. Jolles, C. G. Newton, Eds. (Academic Press, New York, 1995), pp. 89–118.
7. D. M. Shotton and H. C. Watson, *Nature* **225**, 811 (1970).
8. Both the aminimide and the dipeptide inhibitor were prepared by total synthesis and confirmed by infrared spectroscopy (IR), ^{1}H nuclear magnetic resonance (NMR), ^{13}C NMR, and high-resolution mass spectroscopy. Aminimides can be synthesized readily in high yield by easily automated procedures (J. C. Hogan Jr., international patent PCT/US93/0624).
9. We measured rates in aqueous solutions containing 0.1 M Hepes (pH 7.5), 0.5 M NaCl, 10 μM HCl, and 10% dimethyl sulfoxide (DMSO), using either MeO-Suc-Ala-Pro-Val-PNA (where Me is a methyl group, Suc is succinyl, and PNA is *p*-nitroanilide) or Suc-$(Ala)_3$-PNA as substrate. TLMI has a value for K_i of 26 μM, but for the Leu-Phe dipeptide, no measurable inhibition could be obtained at the maximum solubility of 20 μM. Although the aminimide inhibitor is soluble in water at this concentration, DMSO was used for consistency with earlier studies.
10. PPE (Worthington Biochemicals; 96.5% pure) was used without further purification. A 4 mM (200x K_i) stock solution of the aminimide inhibitor in acetonitrile was prepared. Elastase crystals were grown as described [L. Sawyer *et al.*, *J. Mol. Biol.* **118**, 137 (1978)]. Crystals of PPE were transferred to 1 ml of mother liquor (30 mM sodium sulfate and 10 mM sodium acetate, pH 5.0). Slowly, 50 μl of the aminimide inhibitor solution was added. Twenty-four hours later, an additional 50 μl was added. The crystal was mounted in a sealed quartz capillary tube.
11. C. Mattos, D. A. Giammona, G. A. Petsko, D. Ringe, *Biochemistry* **34**, 3193 (1995).
12. W. Bode *et al.*, *EMBO J.* **5**, 2453 (1986).
13. The program X-PLOR [A. T. Brünger, M. Karplus, G. A. Petsko, *Acta Cryst* **A45**, 50 (1989)] was used for refinement. The initial protein model was an unpublished structure of native elastase that had been refined to an *R* factor of 17.8% at 1.6 Å resolution. An initial rigid body refinement of this model with water and bound ions removed, followed by positional refinement, gave an *R* factor of 25.9% against all measured data for the PPE-TLMI complex. An electron density map with coefficients $2F_o$ (observed) $- F_c$ (calculated) was calculated, and protein side chains were adjusted. Electron density indicating the presence of inhibitor bound in the active site was seen. Another round of positional and independent *B* factor refinement was performed, and 122 water molecules, one sulfate ion, and one calcium ion were added to the model. After an additional round of refinement, a model of the inhibitor was added to the protein model on the basis of a difference electron density map with coefficients $F_o - F_c$. The electron density clearly showed the position of the TFA, Leu, and the Iso. portions of the inhibitor. Electron density for the carbonyl group uniquely positions the backbone of the inhibitor in the region of the MBA residue. The orientation of the methyl group on the quaternary nitrogen, which determines the chirality of that nitrogen, was initially unclear in the electron density map. Therefore, a model of the *S* isomer was used in a conformation in which the methyl group was eclipsed with the carbonyl oxygen of the Leu residue. Because this model did not refine well, the alternate conformation was tried in which the methyl group was placed trans to the carbonyl oxygen. This operation converts the *S* isomer into the *R* isomer. This model fitted the observed electron density better and refined smoothly. This result implies that the *R* configuration at this nitrogen is the preferred conformation that binds to the enzyme. Subsequently, several additional rounds of refinement added and removed water molecules. To check on the proper placement of the inhibitor in later stages of refinement, the inhibitor atoms were removed from the model and the model bias was removed from the phases with the program SHAKEUP (A. Lavie, K. N. Allen, R. L. Rardin, personal communication). Subsequent positional and *B* factor refinements followed by difference electron density map calculations indicated that the inhibitor had been placed correctly. The final *R* factor is 19.2% for a model that contains 1829 protein atoms, 1 calcium ion, 1 sulfate ion, and 134 water molecules plus the TLMI inhibitor.
14. All sequence numbering is sequential numbering in elastase.
15. C. Mattos, B. Rasmussen, X. Ding, G. A. Petsko, D. Ringe, *Nature Struct. Biol.* **1**, 55 (1994).
16. C. Mattos and D. Ringe, in *QSAR in Drug Design: Theory, Methods and Applications*, H. Kubinyi, Ed. (ESCOM Science Publishers, Leyden, Netherlands, 1993), pp. 226–254.
17. I. L. de la Sierra, E. Papamichael, C. Sakrellos, J.-L. Dimicoli, T. Prangé, *J. Mol. Recognit.* **3**, 36 (1990). The atomic coordinates of this structure were taken from the Brookhaven Protein Databank [F. C. Bernstein, T. F. Koetzle, G. J. B. Williams, E. F. Meyer Jr., *J. Mol. Biol.* **112**, 535 (1977)].
18. W. Kabsch, *J. Appl. Crystallogr.* **21**, 916 (1988).
19. Abbreviations for the amino acid residues are as follows: A, Ala; C, Cys; D, Asp; E, Glu; F, Phe; G, Gly; H, His; I, Ile; K, Lys; L, Leu; M, Met; N, Asn; P, Pro; Q, Gln; R, Arg; S, Ser; T, Thr; V, Val; W, Trp; and Y, Tyr.
20. P. J. Kraulis, *J. Appl. Crystallogr.* **24**, 946 (1991).

21. Research was supported (in part) by the Biophysics Program at Brandeis University (NIH T32GMO7596) and the Lucille P. Markey Charitable Trust. E.P. was supported by a grant from the Goldwyn Fund at Brandeis University. We thank W. Carlson for helpful discussions and critical reading of this manuscript.

23 December 1994; accepted 3 May 1995

Rational Design of Peptide Antibiotics by Targeted Replacement of Bacterial and Fungal Domains

Torsten Stachelhaus, Axel Schneider, Mohamed A. Marahiel*

Peptide synthetases involved in the nonribosomal synthesis of peptide secondary metabolites possess a highly conserved domain structure. The arrangement of these domains within the multifunctional enzymes determines the number and order of the amino acid constituents of the peptide product. A general approach has been developed for targeted substitution of amino acid–activating domains within the *srfA* operon, which encodes the protein templates for the synthesis of the lipopeptide antibiotic surfactin in *Bacillus subtilis*. Exchange of domain-coding regions of bacterial and fungal origin led to the construction of hybrid genes that encoded peptide synthetases with altered amino acid specificities and the production of peptides with modified amino acid sequences.

Peptide secondary metabolites produced by microoganisms exhibit diversity with respect to chemical structure and biological activity. These metabolites include antibiotics, enzyme inhibitors, plant and animal toxins, and immunosuppressants and therefore are of importance to medicine, agriculture, and biological research (*1*). Two mechanisms of amino acid incorporation into the bioactive peptides have been identified. The multicyclic lantibiotics, for example, are synthesized ribosomally from gene-encoded peptide precursors, which are extensively modified by complex posttranslational processing (*1*). Other peptides are synthesized on protein templates by a nonribosomal mechanism. This group contributes to the structural diversity of peptide secondary metabolites. These peptides may be composed of linear, cyclic, or branched peptide chains and may contain D-, hydroxy-, or *N*-methylated amino acids that may be modified by acylation or glycosylation (*1*, *2*).

Common to these peptides is their mode of synthesis by multifunctional enzymes that use a thiotemplate mechanism and differ in substrate specificity and size (*2*–*6*). Distinct domains represent the functional building units of these multifunctional enzymes that are responsible for specific amino acid activation (including adenylation and thioester formation), modification, and peptide bond

Biochemie/Fachbereich Chemie, Philipps-University of Marburg, D-35032 Marburg, Germany.

*To whom correspondence should be addressed.